



## XAS/EXAFS studies of Ge nanoparticles produced by reaction between $Mg_2Ge$ and $GeCl_4$

Andrew J. Pugsley<sup>a</sup>, Craig L. Bull<sup>b</sup>, Andrea Sella<sup>a</sup>, Gopinathan Sankar<sup>a</sup>, Paul F. McMillan<sup>a,\*</sup>

<sup>a</sup> Department of Chemistry and Materials Chemistry Centre, University College London, 20 Gordon Street, London WC1H 0AJ, UK

<sup>b</sup> SUPA, School of Physics and Astronomy and Centre for Science at Extreme Conditions, University of Edinburgh, Mayfield Road, EH9 3JZ, UK

### ARTICLE INFO

#### Article history:

Received 18 February 2011

Received in revised form

2 June 2011

Accepted 20 June 2011

Available online 28 June 2011

#### Keywords:

Nanoparticles

Metathesis reaction

X-ray absorption spectroscopy

### ABSTRACT

We present results of an XAS and EXAFS study of the synthesis of Ge nanoparticles formed by a metathesis reaction between  $Mg_2Ge$  and  $GeCl_4$  in diglyme (diethylene glycol dimethyl ether). The progress of the formation reaction and the products formed at various stages in the processing was characterised by TEM and optical spectroscopy as well as *in situ* XAS/EXAFS studies using specially designed reaction cells.

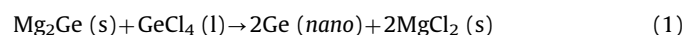
© 2011 Elsevier Inc. All rights reserved.

### 1. Introduction

Semiconducting nanoparticles are well developed for applications ranging from biomedical and environmental sensors to energy-producing devices. Most work to date has focused on II–VI semiconductor systems such as CdS and CdSe that have bandgaps and luminescent properties that vary systematically with nanoparticle size [1–8]. One main reason for the rapid development of these materials is the existence of convenient solution chemistry routes to produce the luminescent nanoparticles *via* arrested precipitation reactions, combined with the ready availability of soluble precursors [9–13]. Following synthesis, the nanoparticles are “capped” with organic groups in solution to terminate, stabilise and functionalise the surface and facilitate their incorporation into devices. Less progress has been made in developing routes to analogous nanoparticles based on well-known group 14 semiconductors such as Si or Ge. In bulk form these materials provide indirect-gap semiconductors that only exhibit significant optical absorption or luminescent properties well above the bandgap energy. However, nanocrystalline as well as amorphous varieties exhibit light absorption and photoelectric energy conversion throughout the IR-visible range [14–24]. Because of the compatibility of these materials with existing semiconductor technology it is important to develop routes to the nanoparticle synthesis [25–34].

A convenient route to produce Si/Ge nanoparticles suspended in organic liquids such as diglyme (diethylene glycol dimethyl

ether) has been described [35–40]. The nanoparticle formation proceeds *via* metathesis/comproportionation reactions between soluble molecular  $SiCl_4$  or  $GeCl_4$  that provide a source of electro-positive  $Si^{4+}$  or  $Ge^{4+}$ , and anionic  $Si^-$ ,  $Ge^{4-}$  species present within solid state Zintl compounds such as NaSi or  $Mg_2Ge$  containing polyanionic units (e.g.,  $Si_4^{4-}$  tetrahedra) [41–43]. Once in colloidal suspension the resulting Si or Ge nanoparticles are transferred to organic solvents such as hexane to carry out capping reactions [35–38]. This type of reaction is being developed as a general approach to provide various capped and core-shell Si/Ge semiconductor-oxide nanoparticles [37,38,44]. It is important to characterise the reaction conditions leading to production of the nanoparticles and their chemical and physical state. Here we used X-ray absorption spectroscopy (XAS) implemented at the Ge K edge [45–50] to study the reaction between  $Mg_2Ge$  and  $GeCl_4$  in diglyme, that produces luminescent Ge nanoparticles within a 2–10 nm size range [35–40]:



### 2. Experimental methods

#### 2.1. Synthesis

All chemical manipulations were carried out in dry  $N_2$  using glovebox and Schlenk line techniques ( $< 1$  ppm  $O_2/H_2O$ ). Liquid  $GeCl_4$  (Acros, 99.99%), was used as received. Crystalline  $Mg_2Ge$  was prepared by heating a stoichiometric mixture of Mg (Aldrich, 99+%) and Ge (Aldrich, 99.999+%) contained in Ta foil and sealed

\* Corresponding author.

E-mail address: [p.f.mcmillan@ucl.ac.uk](mailto:p.f.mcmillan@ucl.ac.uk) (P.F. McMillan).

in a silica tube at 650 °C (3 days): the material was confirmed by powder X-ray diffraction (Siemens D8;  $\text{CuK}\alpha$  radiation) and Raman spectroscopy (Renishaw InVia : 514 nm laser excitation) to be single phase (Fig. 1a).

Diglyme (diethylene glycol dimethyl ether) was obtained from Aldrich (99.5%). As received it was determined to contain  $\sim 400$  ppm  $\text{H}_2\text{O}$  by Karl–Fischer titration. It was found to be critically important to remove all traces of moisture to avoid side reactions between  $\text{GeCl}_4$  and  $\text{H}_2\text{O}$ . In our early experiments the solvent was stirred for 12–48 h over Na/K alloys (Na: Aldrich, 99.95%; K: Fischer, 99.95%) followed by vacuum distillation that was thought to provide sufficient drying. However, EXAFS experiments and TEM results indicated  $\text{GeO}_2$  nanoparticles were produced along with the *nano*-Ge particles. Subsequent Karl–Fischer titrations showed that even such “fully dried” solvents could contain up to  $\sim 250$  ppm of  $\text{H}_2\text{O}$ , that was either incompletely removed initially or re-introduced during subsequent manipulations. After further experimentation we found it was necessary to maintain the  $\text{H}_2\text{O}$  content below 30 ppm by refluxing the solvent over Na for 7–14 days followed by distillation under  $\text{N}_2$  and storage over a Na mirror. We also replaced the air-tight syringes used in early experiments for liquid transfer into the reaction chamber by cannula/septum techniques.

We followed the Ge nanoparticle synthesis procedures reported earlier [35,36].  $\text{Mg}_2\text{Ge}$  (46 mg, 0.38 mmol) was placed in a two-necked 500 ml round-bottom flask along with 100 ml of dried diglyme. The mixture was stirred magnetically and heated to reflux ( $\sim 155$ – $160$  °C) overnight under dry  $\text{N}_2$  to give a grey suspension. SEM examination showed the solid particles broke up into 0.1–0.5  $\mu\text{m}$  fragments and the X-ray diffraction peaks became broadened, indicating structural disorder or nanoparticle formation. We found no evidence for dissolution of the Zintl phase in the liquid but *in situ* XAS experiments indicated the presence of  $\text{Mg}_2\text{Ge}$  particles suspended in the beam path.

$\text{GeCl}_4$  (Aldrich 99.99%: 0.13 ml, 1.14 mmol) was then added to the stirred diglyme– $\text{Mg}_2\text{Ge}$  suspension. This amount corresponds to a 3-fold excess over the stoichiometric amount required for reaction (1): that requirement was suggested previously to be an important condition for successful synthesis [35,36]. After a few minutes the grey  $\text{Mg}_2\text{Ge}$  suspension became clear and the colour changed to light golden-yellow, indicating the formation of Ge nanoparticles. White wispy filaments identified as  $\text{MgCl}_2$  were also formed during the reaction (1). The Ge nanoparticles were then capped by adding excess butyllithium (BuLi: Aldrich, 2.5 M solution in hexane) to the cooled reaction mixture. Excess BuLi was removed by addition of deionised water. The contents were transferred to a separating funnel and the capped Ge nanoparticles extracted into hexane. The non-aqueous phase was washed with deionised water to remove LiCl. After removal of hexane by rotary evaporation, an aliquot of the capped nanoparticles was resuspended in  $\text{CDCl}_3$  for  $^1\text{H}$  NMR spectroscopy using a Bruker AMX-300 instrument. Peaks at  $\delta=1.35$  and 1.52 ppm indicated the presence of Ge-alkyl species in the liquid or perhaps attached to the surface of the nanoparticles. Intense blue photoluminescence characteristic of Ge nanoparticles with a 2–4 nm size range was observed first by UV lamp (365 nm) illumination and then recorded spectroscopically using 325 nm laser excitation during room temperature photoluminescence studies (Fig. 2).

## 2.2. Transmission electron microscopy

We examined the nanoparticles produced at various stages during the experiments using transmission electron microscopy (TEM) combined with selected area diffraction (SAD) and energy-dispersive X-ray (EDX) or electron energy loss (EELS) analysis. Samples were prepared by placing drops on an amorphous C film

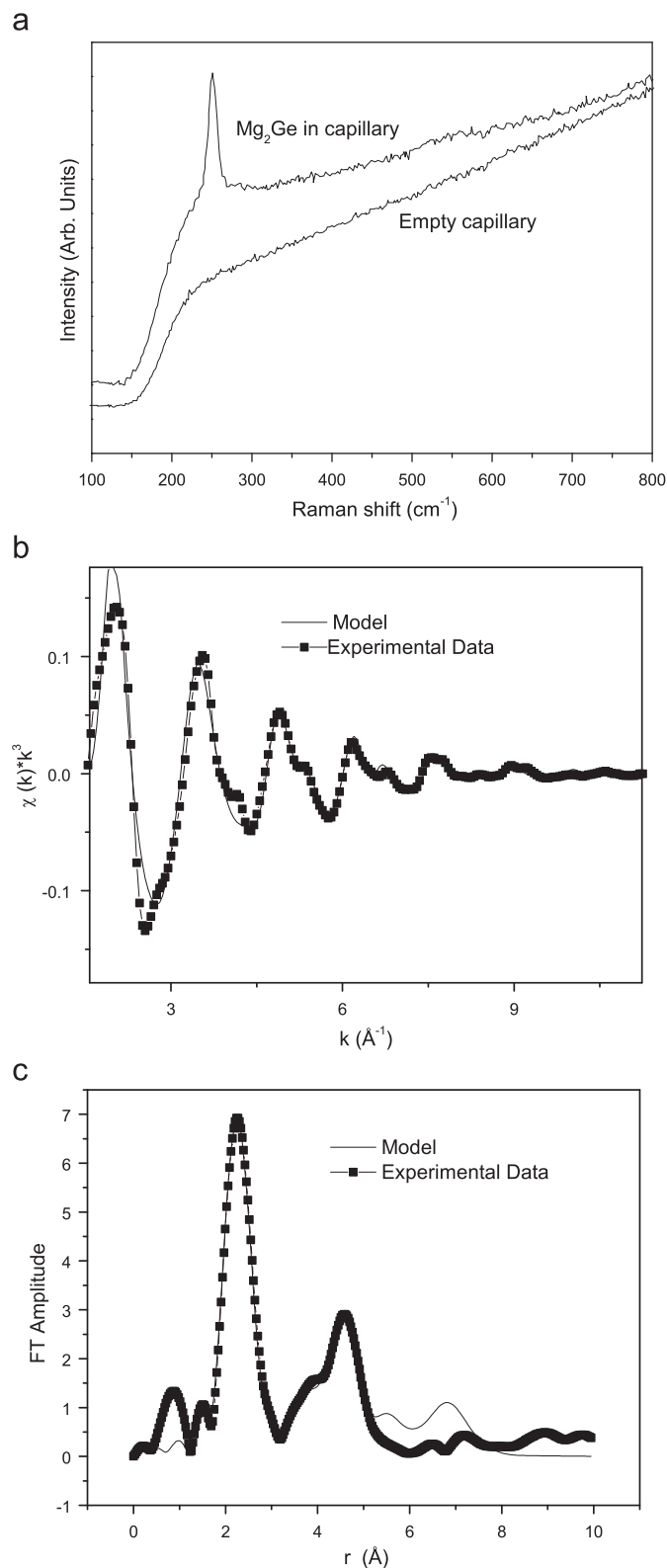


**Fig. 1.** Characterisation of the Zintl phase compound  $\text{Mg}_2\text{Ge}$  used as a precursor for the *nano*-Ge synthesis experiments. (a) Raman spectrum showing the single triply degenerate mode expected for the antifluorite structure (b) Background subtracted EXAFS spectrum at the Ge K edge. (c) Fourier transformed EXAFS data. In (b) and (c) the solid line represents a best fit to the data using a multiple scattering model ( $r$ -value 7%).

supported by a 400 mesh Cu grid and allowing to dry at room temperature. TEM imaging and SAD experiments were carried out using a 100 kV JEOL JEM-100CX11 at UCL or a 300 kV JEOL

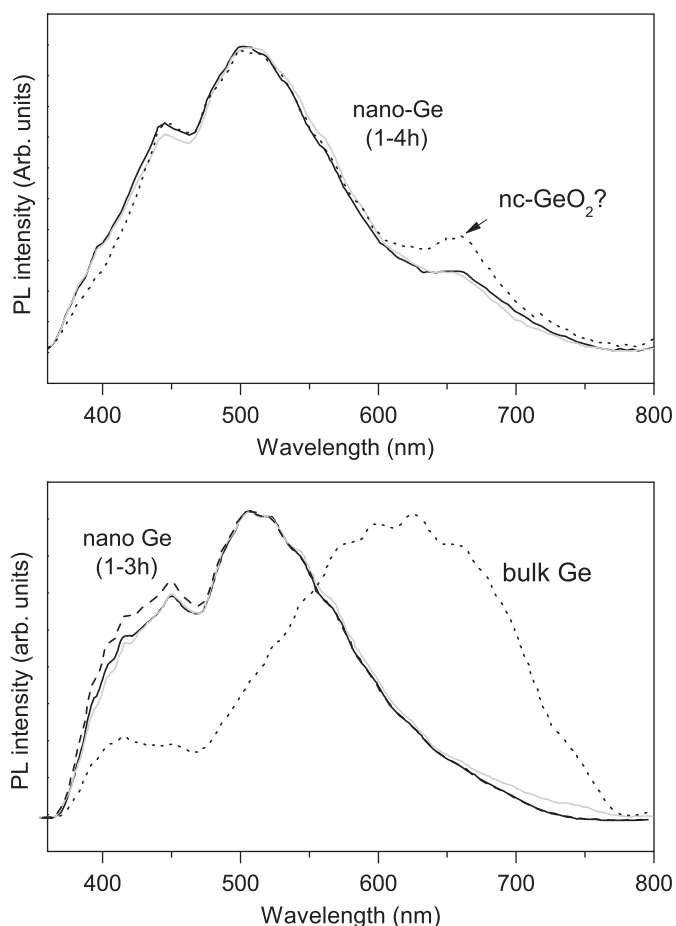


**Fig. 2.** Room temperature photoluminescence spectra of capped Ge nanoparticles in suspension in diglyme following reaction (1) or after extraction into hexane using 325 nm laser excitation show strong features in the 400–550 nm range. (a) Products of an early synthesis containing nanocrystalline q-GeO<sub>2</sub> in addition to *nano*-Ge. (b) Later samples prepared in fully dried diglyme, compared with the PL spectrum of bulk Ge obtained under similar conditions.

JEM-3010 at University of Southampton (Dr. B.A. Cressey). Energy dispersive analyses were performed using a JEOL JEM-2200FS operating at 200 kV in the Department of Materials, Imperial College London (Drs. D. McComb and I. Khan): these measurements revealed the presence of oxygen impurities (K edge  $\sim 0.5$  keV) among samples prepared during the early part of our study and this was confirmed by EELS at the University of Leeds. Later samples showed no presence of oxygen.

### 2.3. XAS/EXAFS measurements

A first series of XAS/EXAFS studies were carried out at the Ge K edge ( $\sim 11.1$  keV) to characterise various solid and liquid state standards and precursor materials to help interpret the nanoparticle formation data. We then examined aliquots removed from the reaction mixtures after various times, and also carried out *in situ* XAS/EXAFS studies while implementing the synthesis reaction (1) using one of a series of specially designed chemical reaction cells. XAS studies were carried out at stations 9.2, 9.3 and 16.5 at SRS Daresbury, UK [51] and also at BM26 (Dutch-Belgian Beamline DUBBLE, BM26, ESRF Grenoble [52]). Double crystal Si(2 2 0) or Si(1 1 1) monochromators were used, slightly detuned to give 50% harmonic rejection in the incident beam. Transmission spectra were obtained using Ar/He-filled ion chambers before and after the sample chamber for  $I_0$  and  $I_t$  measurements. The *in situ* reaction studies were carried out using fluorescence

detection with a solid state Ge detector because of the low concentrations of reactants and products present. Edge positions were calibrated using crystalline Ge and are reported as threshold energies at the maxima in first derivative spectra of the X-ray absorption vs. energy [50]. A “Quick EXAFS” mode was used to achieve rapid collection times (400 s/scan) for *in situ* reaction experiments at SRS 9.2. Similar rapid scan experiments at ESRF BM26 were run using 840 s collection times for each spectrum. Spectra of the solid-state materials were obtained in transmission mode using finely ground materials mounted on tape in the beam path. A special cell with 25 mm mica windows and 2 mm path length was constructed to hold air-sensitive liquids including GeCl<sub>4</sub> in diglyme solution and GeBu<sub>4</sub> in hexane for transmission or fluorescence XAS/EXAFS measurements at both facilities.

*In situ* reaction studies were carried out using various generations of a specially designed high-temperature reaction cell, that enabled stirring the Mg<sub>2</sub>Ge precursor with diglyme under H<sub>2</sub>O-free conditions, addition of GeCl<sub>4</sub> to the reaction mixture, maintaining controlled temperature under reflux and avoiding loss of volatile materials from the reaction mixture [53]. These cells were generally constructed from aluminium block: the sample chamber consisted of a 2 cm diameter hole drilled to a depth of 18 cm along the long axis of the cell. Two 1 cm openings drilled half-way up the cell and closed with 25  $\mu$ m Kapton or mica windows permitted XAS measurements. In later versions Al tubing wrapped with a Cu cooling coil added above the reaction cell provided a condenser for volatile components under reflux conditions: this was connected to a dry N<sub>2</sub> supply and bubbler to exclude ingress of atmospheric O<sub>2</sub>/H<sub>2</sub>O. Electrical cartridge heaters were inserted into holes drilled in the cell body parallel to the sample chamber and  $T$  was monitored using a K-type thermocouple. Cells for *in situ* reaction studies were brought to the synchrotron beamlines pre-sealed and loaded with solid Mg<sub>2</sub>Ge (5.4 mg, 0.04 mmol), diglyme ( $\sim 7$  ml) and a 3 mm magnetic stirrer follower. Liquid GeCl<sub>4</sub> was added using a gas-tight syringe or cannula and the nanoparticle formation reaction (1) was initiated by heating the cell to 155  $^{\circ}$ C.

Normalisation and background procedures to treat the XAS/EXAFS data were mainly carried out using programmes from Daresbury SRS: Excalib, Exback, Exspline, Exbrook, etc. EXAFS modelling was carried out using Excurve98 using theoretical potentials and phase shifts to fit the first three shells with coordination numbers  $N$  around the central atom, radial distances ( $r_{ij}$ ) and Debye–Waller factors. EXAFS studies of solid Mg<sub>2</sub>Ge indicated the importance of including multiple scattering paths modelled using FEFF and IFEFFIT (Fig. 1b and c) [54,55].

EXAFS analyses of our first *in situ* data sets obtained during the nanoparticle formation reaction showed a peak due to Ge–Ge first-neighbour distances that was observed to grow near 2.4  $\text{\AA}$ , as expected (Fig. 3). However, the EXAFS patterns were dominated by a strong peak at 1.7–1.9  $\text{\AA}$  that was assigned to Ge–O oscillations of quartz-structured GeO<sub>2</sub> (q-GeO<sub>2</sub>) nanoparticles present in the samples. These had been produced along with the *nano*-Ge particles because of H<sub>2</sub>O present within the reaction mixture, at concentrations of 200–400 ppm. In our later experiments we used fully dried diglyme (with  $< 30$  ppm H<sub>2</sub>O) and improved reaction cell design as well as modified transfer procedures, so that moisture ingress was controlled or eliminated, and GeCl<sub>4</sub> loss was avoided during the nanoparticle formation reaction.

## 3. Results and discussion

### 3.1. TEM and photoluminescence studies

Nanoparticle size distributions were determined by direct measurement of  $\sim 500$  particles from each of several TEM images

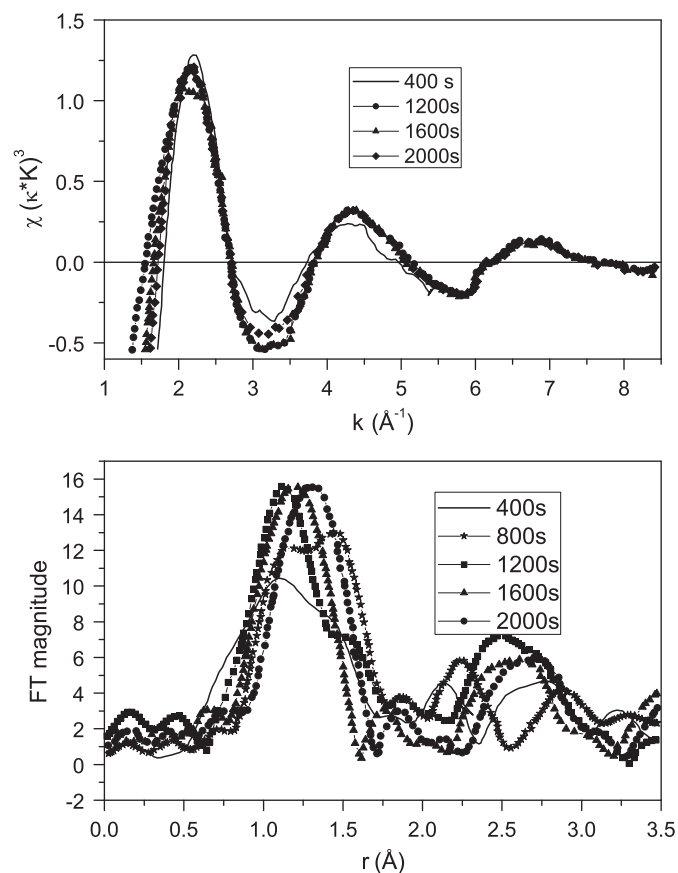


**Fig. 3.** (a) Background subtracted EXAFS region of Ge K-edge XAS spectra in the reaction cell as a function of time (SRS 9.2). The corresponding Fourier transforms of the EXAFS data are shown below. These experiments were carried out in completely dried solvent. The main feature in the FT EXAFS is due to GeO<sub>2</sub> nanoparticles (quartz structure) formed by reaction between GeCl<sub>4</sub> and H<sub>2</sub>O present within the solvent or introduced into the cell during transfer procedures. The growth of a peak near 2.5 Å is apparent due to formation of *nano*-Ge particles.

obtained from samples during the runs (Fig. 4). In a first series of samples, after 1 h the particle size range extended from 1.5 to 4.5 nm, with a mean value near 2.7 nm; after 3 h, the average size had increased to 2.9 nm and to ~3.7 nm by 6 h, with only a few larger particles extending up to ~6 nm in dimension. This direct counting method can underestimate the numbers of the smallest particles because they are often difficult to locate in the TEM images. Particle size distributions for samples prepared under fully anhydrous conditions were indistinguishable from those of earlier samples that contained some nanocrystalline GeO<sub>2</sub> along with the *nano*-Ge particles.

Previous studies have indicated crystalline lattice fringes present for Ge/Si nanoparticles produced by the same synthesis procedures we have attempted to reproduce here [37]. However, in most of our SAD-TEM studies of capped Ge nanoparticles formed by reaction (1) we could detect only diffuse amorphous diffraction rings with a spacing consistent with *a*-Ge (Fig. 5). Well defined diffraction spots found to be arising from some nanoparticles were determined to be due to *q*-GeO<sub>2</sub>, formed by reaction of GeCl<sub>4</sub> with H<sub>2</sub>O in incompletely dried solvent conditions. In later studies of *nano*-Ge particles formed under fully anhydrous conditions we found the diffraction patterns were not stable under electron beam irradiation. We could not determine if (a) the nanoparticles were initially crystalline but amorphised in the beam; (b) the particles were amorphous but crystallised in the beam; or (c) a mixture of crystalline and amorphous nanoparticles were present immediately following synthesis by reaction (1). In certain cases, crystalline diffraction spots

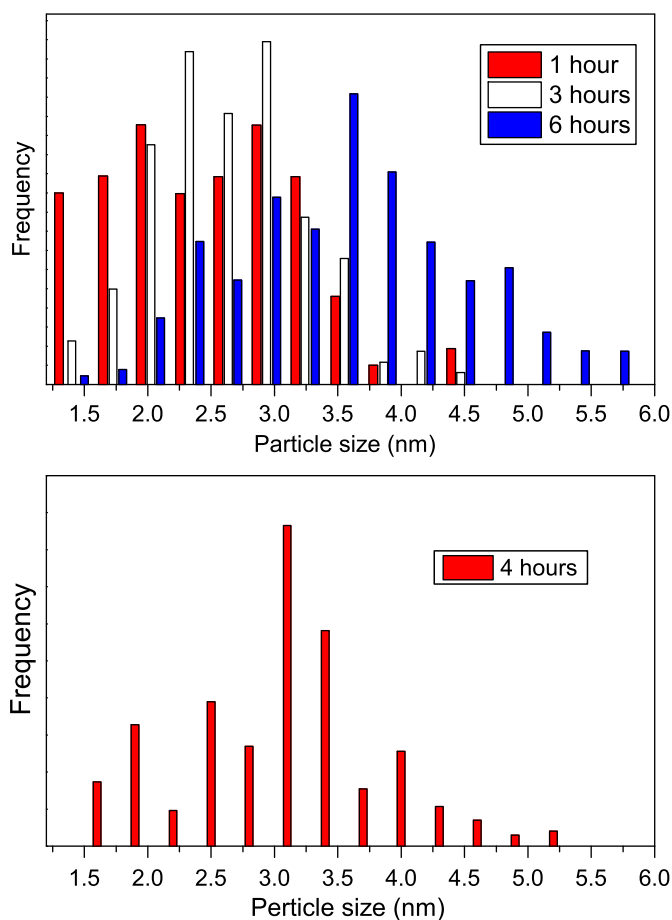


**Fig. 4.** Nanoparticle size distributions determined by direct measurement from TEM images containing ~500 particles. Aliquots were examined for samples removed from the reaction mixtures at 1, 3 and 6 h (above) and after 4 h (below). The first set of samples contained GeO<sub>2</sub> as well as *nano*-Ge particles: the second run was carried out under moisture-free conditions.

were observed during initial exposure of the nanoparticle to the electron beam, using accelerating voltages ranging 100–300 keV; however, these quickly evolved to give amorphous rings within a few seconds of irradiation. In a few cases crystalline spots or sharp rings were also observed to appear during electron beam irradiation of some nanoparticles. Our TEM results could not allow us to conclude if the Ge nanoparticles formed by reaction (1) are amorphous, crystalline or a mixture of both.

The room temperature PL spectra excited by 325 nm laser radiation exhibits a characteristic double maximum at ~430 and ~510 nm, similar to that observed for bulk Ge, but with the lower energy peak displaced to shorter wavelength values (Fig. 2). That corresponds to the blue PL observed in previous studies and under broadband UV irradiation. We did not observe any systematic changes in peak position or the PL intensity as a function of reaction time during our studies as the average particle size evolved between 2 and 4 nm indicated by the TEM results. The PL spectra from samples containing nanocrystalline GeO<sub>2</sub> exhibited an additional weak feature at ~660 nm.

### 3.2. XAS/EXAFS results: model compounds

During our study it was first necessary to interpret the Ge K edge position and XANES to understand the nature of the growing nanoparticles. It is well known that the Ge K edge shifts in response to the bandgap [47,49]. The growing semiconductor nanoparticles are exposed to an O-rich environment within the

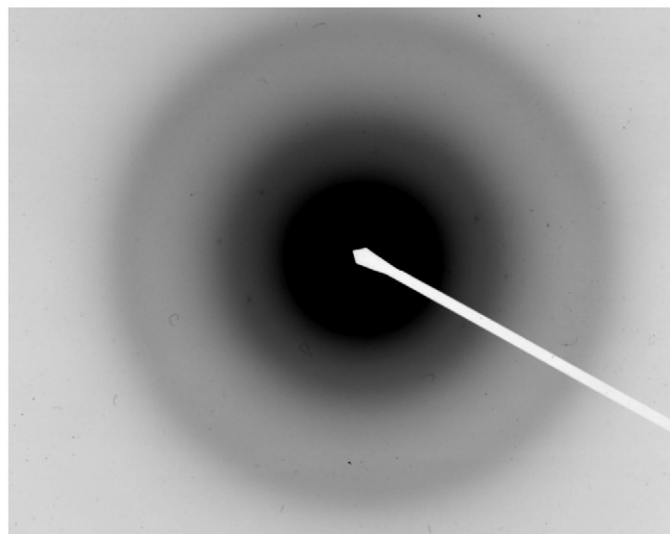
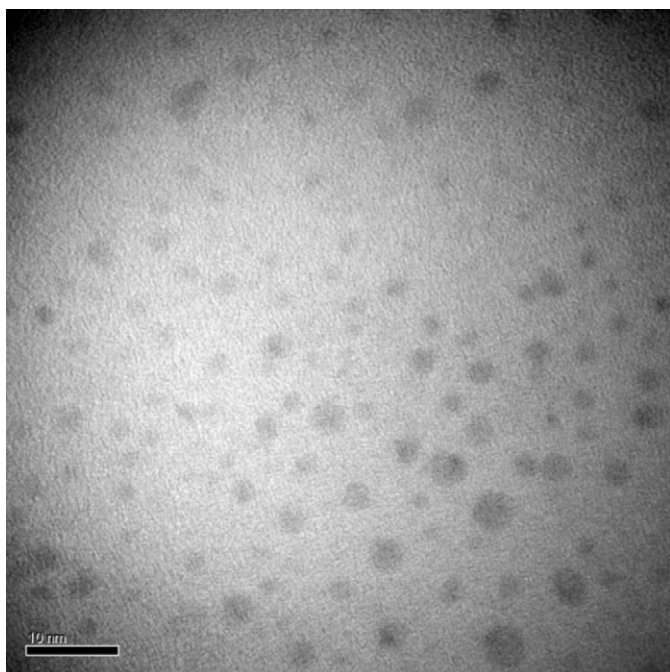


**Fig. 5.** TEM studies of Ge nanoparticles formed by reaction (1). (a) Typical image obtained using the 300 kV JEOL instrument at University of Southampton. The scale bar represents 10 nm. (b) SAD pattern showing the amorphous ring pattern obtained for typical nanoparticles. The ring positions are consistent with diffraction from amorphous Ge. Occasionally, the  $\alpha$ -Ge nanoparticles were observed to recrystallise during electron irradiation; in a few other cases, crystalline spots were observed initially but these disappeared within a few seconds to be replaced by an amorphous pattern.

diglyme solvent, and Ge–C species are expected to appear at the nanoparticle surface after the organic “capping” reaction has taken place, so it was important to characterise changes that could occur as a function of Ge coordination to O- vs C-bearing species. We examined the edge shifts among several solid state materials and molecular compounds containing Ge atoms in different oxidation states and coordination environments to establish correlations that would be useful in our studies of *nano*-Ge particle formation.

The edge position for diamond-structured *c*-Ge occurs at 11103 eV (Fig. 6). The edge crest is broad and it extends to  $\sim$ 11118 eV. Analysis of the EXAFS yields a first-neighbour Ge–Ge distance of 2.451(2) Å in good agreement with X-ray diffraction. Reference spectra for bulk  $\alpha$ -Ge were supplied by Drs. A. Fillipponi (Dip. di Fisica, Univ. degli

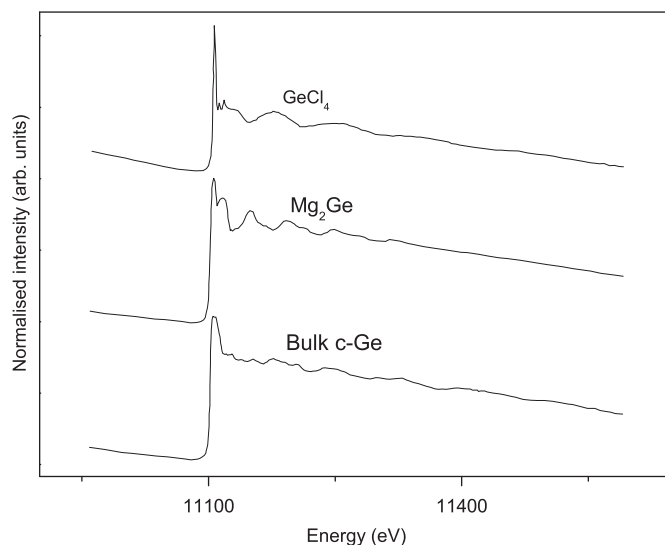


**Fig. 6.** Ge K-edge spectra for  $\text{GeCl}_4$ ,  $\text{Mg}_2\text{Ge}$  and bulk *c*-Ge.

Studi dell' Aquila, Italy) [47] and G. Aquilenti (SISSA, Trieste). The threshold energies for bulk *c*-Ge and  $\alpha$ -Ge are nearly identical: analysis of the EXAFS data for  $\alpha$ -Ge indicates a slightly elongated average Ge–Ge bond length of 2.464(2) Å [47,56–58]. For comparison with the results below, we obtained an XAS spectrum for molecular  $\text{GeBu}_4$  prepared prepared by reacting BuLi with  $\text{GeCl}_4$  in diglyme, representing the Ge-alkyl species that might be formed in side reactions with excess  $\text{GeCl}_4$  present in solution during the capping reaction with BuLi, or existing at the capped *nano*-Ge particle surface. The edge position for this molecular species occurs at 11103 eV, close to the values observed for bulk *c*- and  $\alpha$ -Ge.

The XAS spectrum of molecular liquid  $\text{GeCl}_4$  contains a sharp, characteristic white line with a K-edge value of 11,108 eV (Fig. 6). Sharp oscillations extending to  $\sim$ 120 eV above the edge are due to multiple scattering among Cl–Ge–Cl paths for ejected photoelectrons within the highly symmetric tetrahedral molecules [59]. The solid state Zintl compound  $\text{Mg}_2\text{Ge}$  has an antifluorite ( $\text{CaF}_2$ ) structure with  $\text{Mg}^{2+}$  on tetrahedral sites and  $\text{Ge}^{4-}$  anions on the eight-coordinated sites. During an initial EXAFS analysis we found that a single-scattering model could not reproduce the Fourier-transformed data. We performed a calculation including multiple scattering paths with associated phase and amplitude functions in order to determine the structural parameters, which are in good agreement with those determined by X-ray diffraction methods (Fig. 1). The first neighbour Ge–Mg distance (8-fold coordination) was determined to be 2.7590(4) Å with a Debye–Waller factor 0.0076(2) Å<sup>2</sup>, and the Ge...Ge distance was 4.5427(3) Å (Debye–Waller factor 0.0129(5) Å<sup>2</sup>). Data for phenacite and spinel-structured  $\text{Ge}_3\text{N}_4$  polymorphs have been previously compared with quartz- vs rutile-structured phases of  $\text{GeO}_2$  and provide examples of  $\text{Ge}^{4+}$  in 4- and 6-coordination to O and N with different degrees of covalent bonding [50,60]. Samples of GeS and GeSe containing Ge–Ge and Ge–S, Se bonds within the black phosphorus (LiSi) structure and  $\text{GeSe}_2$  with a tetrahedrally bonded chain structure were also examined and these “standards” have been used in this study to look at the edge effect of covalency and oxidation state.

The edge positions for  $\text{Mg}_2\text{Ge}$  and elemental Ge occur at lower energy than for materials with Ge in positive oxidation states. It has already been proposed that X-ray absorption edge energies are correlated with the effective charge on the absorbing atom or ion [61]. In general, increasing oxidation state is associated with an increase in the partial charge, so that an edge shift to lower energy is expected to occur with lower (i.e., with less positive or

more negative) oxidation states [54]. We plotted the Ge K-edge positions obtained in this study against the formal oxidation states for various compounds relevant to this study (Fig. 7). We find little variation in edge positions among materials with low oxidation state values, but they evolve rapidly towards higher energy values for compounds described by the +4 state. The highest energies occur for the oxides, with the maximum value recorded for octahedrally coordinated rutile-structured *r*-GeO<sub>2</sub>. These results have helped us interpret the XAS data obtained during the nanoparticle formation reactions.

### 3.3. XAS/EXAFS results: nanoparticle synthesis studies

During our early synthesis experiments nanocrystalline GeO<sub>2</sub> was produced along with Ge nanoparticles as a result of small amounts of H<sub>2</sub>O (200–400 ppm) present within the diglyme solvent, or introduced inadvertently into the reaction cell. We first surmised the presence of GeO<sub>2</sub> species from an unexpected peak dominating the EXAFS signal at  $r=1.7\text{--}1.9\text{ \AA}$  (Fig. 4). This could be correlated with the high edge value (11,107 eV) and a sharp edge crest, that is typical for GeO<sub>2</sub>-containing materials (Fig. 9) [50,60]. The edge position and shape were most characteristic of tetrahedrally bonded *q*-GeO<sub>2</sub>, consistent with SAD-TEM results for crystalline nanoparticles in samples quenched from these initial runs.

Later synthesis studies were carried out using fully dried solvent and under anhydrous reaction conditions. The recorded edge position now occurred at a higher energy than that of bulk *c*-Ge or *a*-Ge: the XANES was broadened and was featureless, comparable with the signal for GeBu<sub>4</sub> (Fig. 8). The EXAFS data were dominated by the first shell Ge–Ge peak at 2.45–2.46 Å as expected. No obvious second shell Ge...Ge correlation was observed in the Fourier transformed EXAFS data supporting the likelihood that the nanoparticles formed by reaction (1) are mainly amorphous, in agreement with our TEM results (Fig. 5). A peak at low  $r$  (1.92–1.95 Å) was also present (Fig. 9). This feature could be assigned to Ge–C bonds from species capping the nanoparticles. We determined from TEM studies that the *nano*-Ge particles formed during typical reaction times of 1–6 h had diameters between 2 and 9 nm (20–90 Å) (Fig. 4). The volume (400–380,000 Å<sup>3</sup>) and surface area (1300–25,400 Å<sup>2</sup>) determined for these nanoparticles thus contain 180–16,000 Ge atoms, of

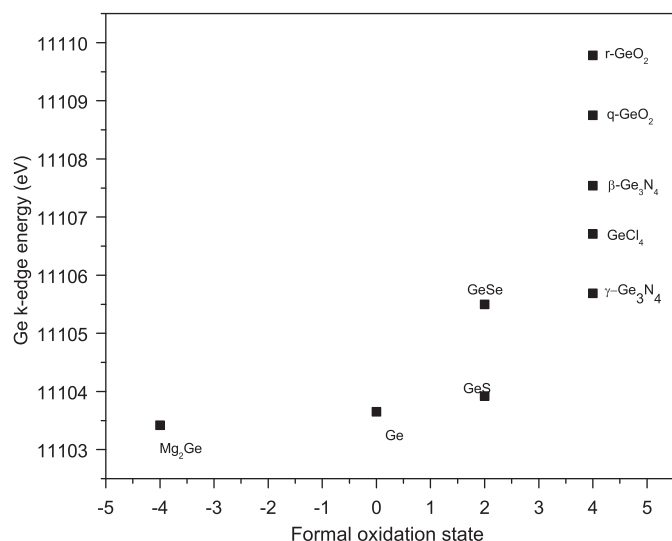


Fig. 7. XAS Ge K edge positions measured for various model compounds plotted against the formal oxidation state.

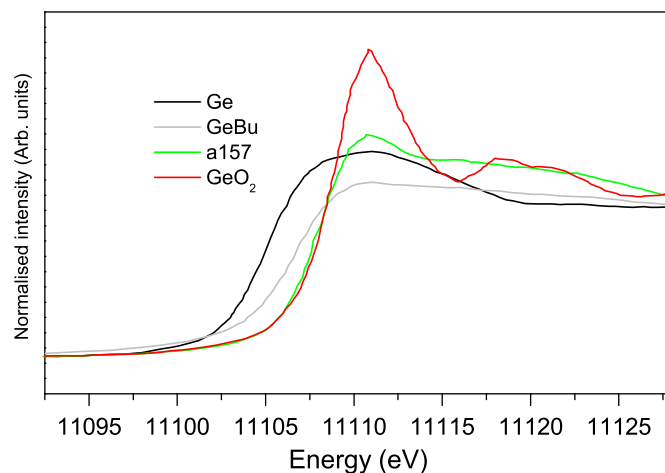
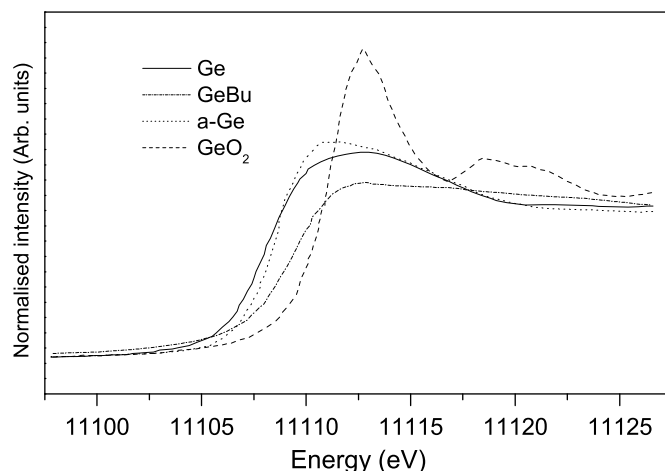


Fig. 8. Characteristic XAS edge spectra for various materials produced during the nanoparticle formation reaction. (a) Comparison of crystalline and amorphous bulk Ge with *q*-GeO<sub>2</sub> and GeBu<sub>4</sub>. (b) Comparison of Ge, GeO<sub>2</sub> and GeBu<sub>4</sub> with a typical aliquot removed from a nanoparticle synthesis run in diglyme (a157).

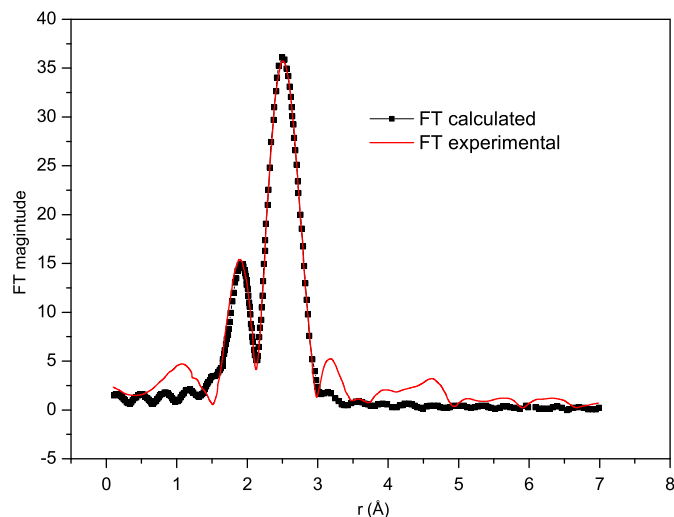


Fig. 9. EXAFS analysis of a typical *nano*-Ge product produced in fully dried diglyme.

which 80–2000 are present at the surface. The ratio of Ge–Ge to Ge–C bonds should then lie between 2:1 and 8:1, within the range observed from the EXAFS data (Fig. 9). However, we also carried out mass spectrometry experiments on samples removed during

the nanoparticle formation reaction following capping by BuLi, and observed characteristic peaks occurring for Ge-alkyl fragments derived from monomeric and oligomeric Ge-butyl species. These were formed by a side reaction occurring between BuLi and excess  $\text{GeCl}_4$  that was present in solution from the initial nanoparticle formation reaction. As noted earlier, previous synthesis studies had indicated that a large (3-fold) excess of  $\text{GeCl}_4$  should be used in the reaction mixture. However, in our present synthesis, none of this reacting species was lost by evaporation, and the solvent was thoroughly dried so no  $\text{GeCl}_4$  was used in forming oxide, and thus the excess remained in solution and was available to react with the capping agent. We then produced  $\text{GeBu}_4$  by reacting  $\text{GeCl}_4$  with BuLi in diglyme solution and obtained its XAS spectrum in which there was only evidence for Ge-alkyl species (i.e., no Ge-Cl remaining). The edge position occurred near 11,103 eV, close to that of bulk *c*- and *a*-Ge, and it has a broad featureless edge crest that is only slightly broader than the solid-state materials (Fig. 8). We conclude that the 1.92–1.95 Å feature observed in the EXAFS data for the Ge nanoparticle samples could contain contributions from both Ge–C bonds formed at the surface of the nanoparticles, and from  $\text{GeBu}_4$  or other Ge-alkyl species present in solution. We could obtain reasonable fits to the observed XAS spectra of various aliquots of our nanoparticle-containing suspensions by taking ~50:50 combinations of contributions from crystalline or amorphous Ge along with  $\text{GeBu}_4$  species (Fig. 10).

We carried out a series of *in situ* reaction studies at ESRF BM26 under anhydrous conditions (Fig. 11). A solution of diglyme and  $\text{Mg}_2\text{Ge}$  was initially stirred at room temperature before the reaction was started and an edge jump was observed which can be attributed to  $\text{Mg}_2\text{Ge}$  particles suspended in the beam path.  $\text{GeCl}_4$  was then added by cannula and the XAS spectrum became dominated by the characteristic sharp edge peak of molecular  $\text{GeCl}_4$ . The heater was then switched on to initiate the nanoparticle formation reaction at 155 °C. Each *in situ* run was carried out for 2–3 h, with each data set accumulated for 840 s (Fig. 11). The contribution of the strong  $\text{GeCl}_4$  signal to the overall XAS decreased rapidly and a new feature grew at low energy signalling the formation of germanium nanoparticles. However, some  $\text{GeCl}_4$  component was still detected in the reaction mixture at up to ~2 h. These preliminary results indicate that *in situ* XAS studies could be used to examine the kinetics and mechanism of the nanoparticle formation reaction.

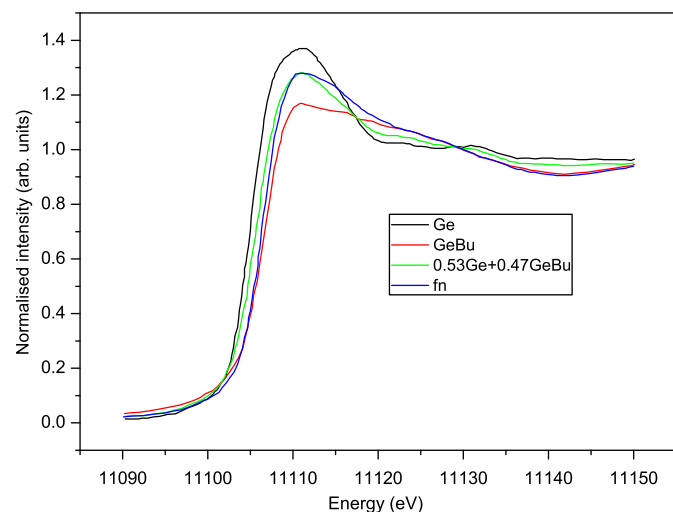


Fig. 10. Result of fitting a typical nanoparticle XAS spectrum ("fn") to a combination of Ge+ $\text{GeBu}_4$  components.

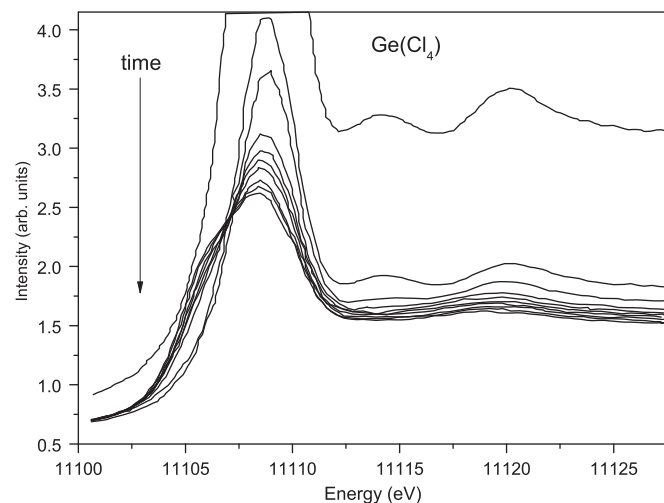


Fig. 11. *In situ* XAS data obtained during the course of reaction (1) using fully dried diglyme and the second generation reaction cell. The first spectrum was taken after  $\text{GeCl}_4$  was added to the cell, before heating to 155 °C to initiate the reaction. The strong white line signal for  $\text{GeCl}_4$  is off scale. Prior to this a signal for  $\text{Mg}_2\text{Ge}$  solid particles stirred into the beam path was observed, but this was obscured by the strong  $\text{GeCl}_4$  spectrum. The sequence of spectra were taken as a function of time after onset of the reaction. Each spectrum was recorded for 840 s during 2.5 h. The strong  $\text{GeCl}_4$  signal diminishes rapidly in intensity as the reaction proceeds. Growth of the feature at low energy (~1105 eV) is observed due to the formation of Ge nanoparticles.

#### 4. Conclusions

We studied formation of *nano*-Ge particles in an organic solvent (diglyme) by a heterogeneous metathesis/comproportionation reaction between dissolved  $\text{GeCl}_4$  ( $\text{Ge}^{4+}$ ) and suspended  $\text{Mg}_2\text{Ge}$  ( $\text{Ge}^{4-}$ ). We have characterised the solid state starting material  $\text{Mg}_2\text{Ge}$  using XAS/EXAFS along with Raman spectroscopy. We noted the formation of nanocrystalline *q*- $\text{GeO}_2$  along with *nano*-Ge during early runs carried out using incompletely dried diglyme solvent: we determined that < 30 ppm  $\text{H}_2\text{O}$  must be maintained throughout the synthesis in order to avoid production of oxide. However, the presence of *nc*-*q*- $\text{GeO}_2$  does not affect the photoluminescence properties. The Ge nanoparticles produced in our studies were mainly amorphous, with average size 2–4 nm for reaction times ranging between 0.5 and 6 h. Our *in situ* XAS/EXAFS experiments offer a new way to monitor and determine the mechanism and kinetics of the nanoparticle formation reaction.

#### Acknowledgments

We thank CCLRC (now STFC) for access to various stations at the SRS (closed since August 2008): also Nick Chinnery, Bob Bilsborrow, C. Corrigan and Mark Jackson for their help with various XAS measurements and sample handling. M. Sheehy (previously at the RI) is thanked for building the initial *in situ* cell within the Davy-Faraday Research Laboratory. The experiments were supported by a Wolfson Foundation-Royal Society Research Merit Award and EPSRC Senior Research Fellowship to PFM (EP/D07357X) and by EPSRC Portfolio award EP/D504782 to PFM in collaboration with CRA Catlow and P Barnes.

#### References

- [1] A.P. Alivisatos, A.L. Harris, N.J. Levinos, M.L. Steigerwald, L.E. Brus, *Journal of Chemical Physics* 89 (1988) 4001–4011.
- [2] L.E. Brus, *Nature* 353 (1991) 301–302.

- [3] D.J. Crouch, S. Norager, P. O'Brien, J.-H. Park, N. Pickett, *Philosophical Transactions of the Royal Society London A* 361 (2003) 297–310.
- [4] D.J. Crouch, P. O'Brien, M.A. Malik, P.J. Skabara, S.P. Wright, *Chemical Communications* (2003) 1454–1455.
- [5] A. Mews, A.V. Kadavanich, U. Banin, A.P. Alivisatos, *Physical Review B* 53 (1996) 13242–13245.
- [6] P. O'Brien, *Current Opinion in Solid State and Materials Science* 6 (2002) 335.
- [7] R. Rossetti, J.L. Ellison, J.M. Gibson, L.E. Brus, *Journal of Chemical Physics* (1984) 4464–4469.
- [8] R. Rossetti, S. Nakahara, L.E. Brus, *Journal of Chemical Physics* (1983) 1086–1088.
- [9] J.G. Brennan, T. Siegrist, P.J. Carroll, S.M. Stucynski, L.E. Brus, M.L. Steigerwald, *Journal of the American Chemical Society* 111 (1989) 4141–4143.
- [10] P. Lianos, J.K. Thomas, *Chemical Physics Letters* 125 (1986) 299–302.
- [11] T. Dannhauser, M. O'Neil, K. Johansson, D. Whitten, G. McLendon, *Journal of Physical Chemistry* 90 (1986) 6074–6076.
- [12] A. Fojtik, H. Weller, U. Kock, A. Henglein, *Berichte der Bunsengesellschaft fuer Physikalische Chemie* 88 (1984) 969–977.
- [13] L. Spanhel, M. Haase, H. Weller, A. Henglein, *Journal of the American Chemical Society* 109 (1987) 5649–5655.
- [14] A.P. Alivisatos, *Science* 271 (1996) 933–937.
- [15] K. Brunner, *Reports on Progress in Physics* 65 (2002) 27–72.
- [16] L.E. Brus, P.F. Szajowski, W.L. Wilson, T.D. Harris, S. Schuppler, P.H. Citrin, *Journal of the American Chemical Society* 117 (1995) 2915–2922.
- [17] R.T. Collins, P.M. Fauchet, M.A. Tischler, *Physics Today* 50 (1997) 24–31.
- [18] M. Larsson, A. Elfving, P.O. Holtz, G.V. Hansson, W.A. Ni, *Surface Science* 532 (2003) 832–836.
- [19] K.A. Littau, P.J. Szajowski, A.J. Muller, A.R. Kortan, L.E. Brus, *Journal of Physical Chemistry* 97 (1993) 1224–1230.
- [20] S. Miyazaki, K. Sakamoto, K. Shiba, M. Hirose, *Thin Solid Films* 255 (1995) 99–102.
- [21] M. Nirmal, L.E. Brus, *Accounts of Chemical Research* 32 (1999) 407–414.
- [22] T. Suemoto, K. Tanaka, A. Nakajima, T. Itakura, *Physical Review Letters* 70 (1993) 3659–3662.
- [23] J.C. Vial, A. Bsiesy, F. Gaspard, R. Herino, M. Ligeon, R. Muller, R. Romestain, *Physical Review B* 45 (1992) 14171–14176.
- [24] L.T. Canham, *Applied Physics Letters* 57 (1990) 1046.
- [25] H.W. Chiu, C.N. Chervin, S.M. Kauzlarich, *Chemistry of Materials* 17 (2005) 4858–4864.
- [26] H.W. Chiu, S.M. Kauzlarich, E. Sutter, *Langmuir* 22 (12) (2006) 5455–5458.
- [27] J. Cho, *Electrochimica Acta* 54 (2) (2008) 461–466.
- [28] S.J. Kim, O.K. Qu, L.S. Chang, E.A. Stach, C.A. Handwerker, A. Wei, *Journal of Materials Chemistry* 20 (2) (2010) 331–337.
- [29] K.T. Park, H.D. Um, S.W. Jee, J.Y. Jung, Y.C. Park, J.M. Yang, J.H. Lee, *Chemical Vapor Deposition* 14 (11–12) (2008) 331.
- [30] S. Prabakar, A. Shiohara, S. Hanada, K. Fujioka, K. Yamamoto, R.D. Tilley, *Chemistry of Materials* 22 (2) (2010) 482–486.
- [31] A.Y. Shah, A. Wadawale, B.S. Naidu, V. Sudarsan, R.K. Vatsa, V.K. Jain, V. Dhayal, M. Nagar, R. Bohra, *Inorganica Chimica Acta* 363 (14) (2010) 3680–3684.
- [32] H.J. Song, S.M. Yoon, H.J. Shin, H. Lim, C. Park, H.C. Choi, *Chemical Communications* 34 (2009) 5124–5126.
- [33] H.P. Wu, J.F. Liu, M.Y. Ge, L. Niu, Y.W. Zeng, Y.W. Wang, G.L. Lv, L.N. Wang, G.Q. Zhang, J.Z. Jiang, *Chemistry of Materials* 18 (7) (2006) 1817–1820.
- [34] H.P. Wu, J.F. Liu, Y.W. Wang, Y.W. Zeng, J.Z. Jiang, *Materials Letters* 60 (7) (2006) 986–989.
- [35] B.R. Taylor, S.M. Kauzlarich, G.R. Delgado, H.W.H. Lee, *Chemistry of Materials* 11 (1999) 2493–2500.
- [36] B.R. Taylor, S.M. Kauzlarich, H.W.H. Lee, G.R. Delgado, *Chemistry of Materials* 10 (1998) 22–24.
- [37] C.-S. Yang, S.M. Kauzlarich, Y.C. Wang, *Chemistry of Materials* 11 (1999) 3666–3670.
- [38] X. Zhang, D. Neiner, S. Wang, A.Y. Louie, S.M. Kauzlarich, *Nanotechnology* 18 (2007) 095601.
- [39] R.A. Bley, S.M. Kauzlarich, *Journal of the American Chemical Society* 118 (1996) 12461–12462.
- [40] R.A. Bley, S.M. Kauzlarich, H.W.H. Lee, J.E. Davis, in: *Materials Research Society Symposium Proceedings*, vol. 351, 1994, pp. 275–280.
- [41] S.M. Kauzlarich, *Chemistry, Structure, and Bonding of Zintl Phases and Ions*, VCH, New York, 1996.
- [42] R. Nesper, *Progress in Solid State Chemistry* 20 (1990) 1.
- [43] H. Schäfer, *Annual Review of Materials Science* 15 (1985) 1.
- [44] N. Zaitseva, Z.R. Dai, C.D. Grant, J. Harper, C. Saw, *Chemistry of Materials* 19 (2007) 5174–5178.
- [45] B.K. Teo, *EXAFS: Basic Principles and Data Analysis*, Springer-Verlag New York, 1986.
- [46] G.E.J. Brown, G. Calas, G.A. Waychunas, J. Petiau, *Reviews in Mineralogy* 18 (1988) 431–512.
- [47] A. Filippini, A. Di Cicco, *Physical Review B* 51 (1995) 12322–12337.
- [48] E.A. Stern, D.E. Sayers, F.W. Lytle, *Physical Review B* 11 (1975) 4836–4846.
- [49] J. Bläsing, P. Kohlert, M. Zacharias, P. Veit, *Journal of Applied Crystallography* 31 (1998) 589–593.
- [50] L. Bertini, P. Ghigna, M. Scavini, F. Cargnoni, *Physical Chemistry Chemical Physics* (2003). doi:10.1039/b21202h.
- [51] G.N. Greaves, C.C.R. A. G.E. Derbyshire, M.I. McMahon, R.J. Nelmes, G. van der Laan, *Nature Materials* 7 (2008) 827–830.
- [52] S. Nikitenko, A.M. Beale, M.J. van der Eerden, S.D.M. Jacques, O. Leynaud, M.G. O'Brien, D. Detallenaere, R. Kaptein, B.M. Weckhuysen, W. Bras, *Journal of Synchrotron Radiation* 15 (2008) 632–640.
- [53] A.J. Pugsley, *Synthesis of Ge-Naoparticles in Organic Solution: Chemical and Structural Characterisation and In Situ Studies of the Formation Reaction*, Ph.D. Thesis, University College London, 2008.
- [54] M. Newville, B. Ravel, D. Haskel, J.J. Rehr, E.A. Stern, Y. Yacoby, *Physica B* 209 (1995) 154–156.
- [55] J.J. Rehr, J.M. Deleon, S.I. Zabinsky, R.C. Albers, *Journal of the American Chemical Society* 113 (1991) 5135–5140.
- [56] G. Bunker, *Nuclear Instrumentation and Methods* 207 (1983) 437.
- [57] G. Dalba, P. Fornasini, M. Grazioli, F. Rocca, *Journal of Non-Crystalline Solids* 164&166 (1993) 159.
- [58] D.E. Sayers, E.A. Stern, F.W. Lytle, *Physical Review Letters* 27 (1971) 1204.
- [59] C.R. Natoli, D.K. Misemer, S. Doniach, F.W. Kutzler, *Physical Review A* 22 (1980) 1104–1108.
- [60] C.L. Bull, P.F. McMillan, J.-P. Itié, A. Polian, *Physica Status Solidi (a)* 201 (2004) 909–916.
- [61] A. Yoshiasa, T. Tamura, O. Kamishima, K.-I. Murai, *Journal of Synchrotron Radiation* 6 (1999) 1051–1058.